Optical, Vibrational, and Structural Properties of MoS2 Nanoparticles Obtained by Exfoliation and Fragmentation via Ultrasound Cavitation in Isopropyl Alcohol.

UNIVERSITÀ DEGLI STUDI DI TORINO

Journal of Physical Chemistry C

Volume 119, Issue 7, 2015, Pages 3791-3801

DOI: 10.1021/jp511973k

J. Phys. Chem. C, 2015, 119 (7), pp 3791–3801, **DOI:** 10.1021/jp511973k

Optical, Vibrational and Structural Properties of MoS_2 Nanoparticles Obtained by Exfoliation and Fragmentation via Ultrasound Cavitation in Isopropyl Alcohol

*Lucia Muscuso, Sara Cravanzola, Federico Cesano *, Domenica Scarano and Adriano Zecchina.*

Department of Chemistry, NIS (Nanostructured Interfaces and Surfaces) Interdepartimental Centre and INSTM Centro di Riferimento, University of Torino, Via P. Giuria, 7, 10125 Torino (Italy).

KEYWORDS. Few-layer MoS_2, MoS_2 nanoclusters; liquid phase exfoliation; UV-vis and IR spectroscopy; Atomic Force Microscopy; Transmission Electron Microscopy; High Resolution Transmission Electron Microscopy.

ABSTRACT. Thin sheets and MoS_2 nanoparticles have been obtained by exfoliation/fragmentation processes via intense ultrasound cavitation in isopropyl alcohol (IPA). The formation mechanism, the structure, (in terms of size, presence of defects, lattice periodicity) and the optical and vibrational properties of the obtained materials have been investigated by means of Atomic Force (AFM), High Resolution Transmission Electron (HRTEM) Microscopies, UV-vis-NIR (UV-visible Near Infrared) and DRIFT (Diffuse Reflectance Infrared Fourier Transform) spectroscopies. FFT (Fast-Fourier Transform) analyses of HRTEM images have provided a simple and powerful tool to better evidentiate defective situations on extended and regular regions of exfoliated MoS_2 nanosheets with large lateral dimensions. The transparent ultracentrifuged portion of MoS_2 in IPA is characterized by size and height distributions peaking at about 6 and 1,5 nm respectively, a fact which is indicative of very high fragmentation and very reduced staking. The evolution of the UV-Vis-NIR and DRIFT spectra upon increasing sonication time and ultracentrifugation give unprecedented information on the optical properties of nanoparticles, on the vibrational properties of surface species and on the lattice modes of virgin and fragmented material. It is also demonstrated that the extensive layers fragmentation due to the cavitation field is associated with rupture of MoSMo bonds and subsequent exposure of coordinatively and chemically unsaturated Mo and S species. These chemically unsaturated species readily react with the IPA solvent and with atmospheric oxygen with the predominant formation of surface hydroxyl, alkyl and to a lesser extent, oxidized species like sulphate and carbonylic and carboxylate groups. It is so concluded that the edges formed by layers breaking in the IPA solution are fully functionalized. This spectroscopic study is made possible by the complete absence of adsorbed IPA, which being a low boiling solvent, can be easily removed from MoS_2 and do not interfere in the DRIFT measurements. The transparent fraction containing the fragmented particles can be used for blending MoS_2 nanoparticles with high surface area materials. This process is favoured by the volatile character of IPA, which can be easily removed from the ultrasonicated material. This makes the proposed method fully suitable to prepare MoS_2-based hybrid composite materials by simple impregnation of high surface area supports.

1. Introduction.

In the last few years, the interest in exploration of layered materials has paved the way to the synthesis and characterization of graphene, graphene-like materials and their composites.[1-2] Among all transition metal dichalcogenide semiconductors, MoS_2 has attracted a huge interest because of its electronic, optical and catalytic properties,[3-10] as well as for its possible applications in many fields (dry lubrification, nanoelectronics, electrode materials for Li-ion batteries, photovoltaic cells, membranes, photocatalysts, catalysts for hydrodesulfurization, hydrogen evolution and oxygen-reduction).[11-25] Depending on the application fields, two main structures can be considered: regular and large-area MoS_2 monolayers, with unique electronic and optical properties[26-29] and small clusters, quantum dots or "patches" (often defective) made by few-layer MoS_2 of reduced size, which can have enhanced photoluminescence, catalytic, photocatalytic and electrochemical efficiencies.[22-23, 30-35] It is known that, moving from bulk to large area mono-layers to nanoparticles, strong quantum size effects are occurring, which alter the optical properties. In more detail, a three-dimensional confinement of the carriers produces larger energy shifts of the excitons peaks than those due to the one-dimensional (perpendicular to the layer planes) confinement. Such effects are explained with a large increase in the spin-orbit splittings at the top of the valence band at the *K* and *M* points of the Brillouin zone with decreasing cluster size, as well as with changes in the hybridization degree of the orbitals, which make up the states at these points.[36] Therefore, when the clusters size becomes smaller than that of the bulk excitons, we move from band (solid-like) to discrete levels (molecule-like) spectra.

By decreasing also the crystals thickness to a single monolayer, the nature of the band gap also changes from indirect to direct, which accounts for a giant enhancement (about 10^4) of the photoluminescence. This suggests that, by tailoring the band gap, the material may be optimized for photocatalytic and photovoltaic applications.[37] Therefore, in order to fabricate high quality layered structures or differently sized clusters, the size control becomes remarkably significant. Mono or few-layers MoS_2 can be obtained by bottom-up growth methods, including wet chemical synthesis (hydrothermal reactions),[25] chemical vapour deposition,[38-39] or more frequently by top-down approaches (exfoliation) including mechanical,[40-43] chemical (forced hydration of Li-intercalated MoS_2)[15, 44-47] or solution methods.[26, 34, 48-50] The extent of the exfoliation/cleavage processes via acoustic cavitation, together with mechanical and chemical activation (i.e. hot-spot process), is

depending on numerous parameters, especially on the structure, on the nature and type of the solid matter (i.e. crystalline, nanotube, etc.) and on the used solvent, as well as on the ultrasound frequency, power, intensity and sonication times.[51-52] It is well known, that the solvent is affecting the exfoliation process (MoS_2, graphene) in terms of surface tension and Hansen solubility parameters (δ_D ~ 17-19 $MPa^{½}$, δ_P ~6-12 $MPa^{½}$, δ_H ~ 4.5-8.5 $MPa^{½}$).[48, 53-54] For instance, stable dispersions of a large population of mono- or few-layers MoS_2 nanosheets can be generated by adopting appropriate Hansen solubility parameters and a surface tension of ~ 40 mJ/m^2. Among the many solvents, including binary solvents or binary solvent-surfactant mixtures, N-methyl-pyrrolidone (NMP), N-vinylpyrrolidinone (NVP), cyclohexylpyrrolidinone (CHP), dimethylformamide (DMF), are usually employed.[22, 48-50, 53, 55-56]

In general terms the best solvents for MoS_2 exfoliation and stable formation of colloidal suspensions have high boiling points. However, when the scope of exfoliation is the deposition of colloidal particles onto the supports to generate films or supported MoS_2-based catalysts, the difficulty of removing the high boiling solvents can be a problem. On the contrary, the use of low boiling point solvents or solvent mixtures offers some advantages including low cost and easy removal. Kai-Ge Zhou et al.[54] have demonstrated that ethyl alcohol/water mixtures are efficient and volatile solvents for a good dispersion of MoS_2 under sonication.

Generally, a mixture of exfoliated MoS_2 nanosheets with large lateral dimensions, together with nanoparticles few nanometers in sizes, can be obtained via ultrasonication. [23, 35, 46] In fact, the dispersion of layered materials under sonication, which is a highly energetic process, consists of two phenomena.

The first one is the separation of solid into single layer or few layers platelets, where Hansen solubility is playing a dominant role. In principle, with this method single layers of unlimited extension could be obtained. The second phenomenon is the fragmentation of the platelets, which is necessarily associated with the breaking of the MoSMo bridges. The occurrence of this phenomenon is limiting the extension of the platelets up to the point that MoS_2 dots can be potentially generated.

As the breaking of MoS bonds leads to the formation of chemically unsaturated species, the fragments react necessarily with the solvent or with oxygen or both. The terminations of the particles are consequently carrying chemical groups formed during sonication, which in turn play a role in the stabilization of the fragments. Of course the smaller are the particles the larger is the role of edges functionalization. It is expected that the stoichiometric composition of the smallest fragments (dots) formed in solution can be

distinctly different from that of pure MoS_2. This is probably the reason why the MoS_2 dots prepared by means of bottom up methods in presence of sulfur are not stoichiometric and have a Mo/S ratio near to 2.5.[57] To our knowledge, the role of the solvent structure and of the functionalization on the fragmentation caused by sonication has not received a specific attention.

In this work, the effects of the ultrasonication in isopropyl alcohol (green, low boiling point and "poor" solvent, i.e. low specific Hansen solubility)[54] of stoichiometric MoS_2 particles is discussed, with the aim to highlight whether the fragmentation of MoS_2 into small nanoclusters/quantum dots is prevailing, rather than the simple exfoliation (typically occurring in good exfoliation solvent). When the results are compared with those obtained with N-methylpyrrolidone (NMP) (results not discussed in detail for the sake of brevity) we have observed by AFM (Atomic Force Microscopy) and HRTEM (High Resolution Transmission Electron Microscopy) that IPA gives good dispersion and so it makes easy the blending of MoS_2 particles with other materials to give hybrid nanocomposites, which is the ultimate application we are interested in.

In general, it is known that the UV-visible spectra can give relevant information on the nature of the obtained materials (bulk, exfoliated nanosheets or clusters). In particular, it is known that, for exfoliated MoS_2 nanoparticles (nanosheets or clusters) in different solvents, all bands are shifted to shorter wavelengths as compared to those of bulk MoS_2.[23, 46] Therefore, in this study the optical properties of the solutions obtained after increasing sonication time and ultracentrifugation have been studied by means of UV-vis-NIR (UV-visible Near Infrared). Furthermore, as the nature of chemical groups at the particle terminations induced by sonication is another aim of this study, DRIFT (Diffuse Reflectance Infrared Fourier Transform spectroscopy) has been applied. It will be shown that this spectroscopy has great and unexpected potentialities not only in the determination of the vibrational properties of surface species, but also on the characterization of the MoS_2 vibrational models. To investigate the presence of the surface groups, the use of a low boiling solvent, which can be easily removed from the surface, facilitates the investigation because physically adsorbed species are easily removed and do not interfere (unlike solvents characterized by high boiling point).

2. Experimental Methods.

MoS_2 powders (Aldrich) with average particle sizes of ~6 μm were dispersed in isopropyl alcohol (IPA) (2 mg/10 ml) and the dispersion was sonicated at 20KHz for 6 hours by a VCX 500 Sonics Vibracell ultrasonic processor (power 500W) equipped with a Ti alloy tapered microtip (d= 3mm, 30% amplitude). A great intensity of cavitation with a concentrated field can be obtained by the small diameter horn in the restricted volume of the solution, which has been placed in an ice bath to control the temperature during the whole sonication step (6h). The obtained dark-gray and turbid solutions were then centrifuged (30 minutes, 4000 rpm), thus causing the heavy MoS_2 particles to precipitate at the bottom of the centrifuge tube, while the supernatant liquid varies from a clear/transparent yellowish (top) to a more opaque color (middle-down). The "transparent" and "opaque" solutions have been placed, immediately after the centrifugation, inside 10 mm thick quartz cuvettes and have been monitored immediately.

After gently ultrasonication of MoS_2 flakes in a standard bath sonicator able to separate the particles, a MoS_2 film was directly deposited on an optical quartz window, to be used as a reference.

The optical properties of the dispersed solutions have been investigated at room temperature by using a double beam UV-vis-NIR spectrophotometer (Varian Cary UV 5000) operating in the wavelength range of 190-2500 nm and the spectra of the solution have been recorded in transmission mode.

FTIR spectra were collected in air, with a Nicolet 6700 spectrophotometer, equipped with a DRIFT Smart Accessory and a MCT detector. DRIFT spectra were recorded for sonicated, non-centrifuged MoS_2 samples. Each spectrum was collected by using 128 scans at a resolution of 4 cm^{-1}. The reflectance spectra were converted in Kubelka-Munk units. Samples were preventively dried in air at 100°C for 15 h to remove physisorbed isopropanol and the spectra were instantly recorded to avoid the adsorption of undesired molecules.

Morphologies and structures of the MoS_2 nanoparticles have been investigated by means of: a) Atomic Force Microscopy (AFM, Park Systems XE-100) operating in intermittent contact mode and Transmission Electron Microscopy (TEM, JEOL 3010-UHR instrument operating at 300 kV with a point-to point resolution of 0.12 nm and equipped with a 2k×2k pixels Gatan US1000 CCD camera). Due to the strong tendency to aggregate/restack upon deposition, samples for AFM and TEM measurements were first diluted with additional isopropyl alcohol and then the solution dropped on freshly cleaved mica and on copper grids

covered with a lacey carbon film, respectively. Sizes and structures of the crystallographic planes of the MoS_2 particles have been obtained by analyzing more than 250 particles in all systems.

3. Results and Discussion.

3.1 The exfoliation and fragmentation process as studied by HRTEM: from the native to the sonicated material extracted from the bottom of the ultracentrifuged solution.

The effect of a great intensity ultrasound cavitation in isopropyl alcohol has been investigated by HRTEM.

Native MoS_2 flakes have dimensions in the 0.5÷5 μm range along the plane and are about 100 nm in thickness (arrows in Figure 1a).

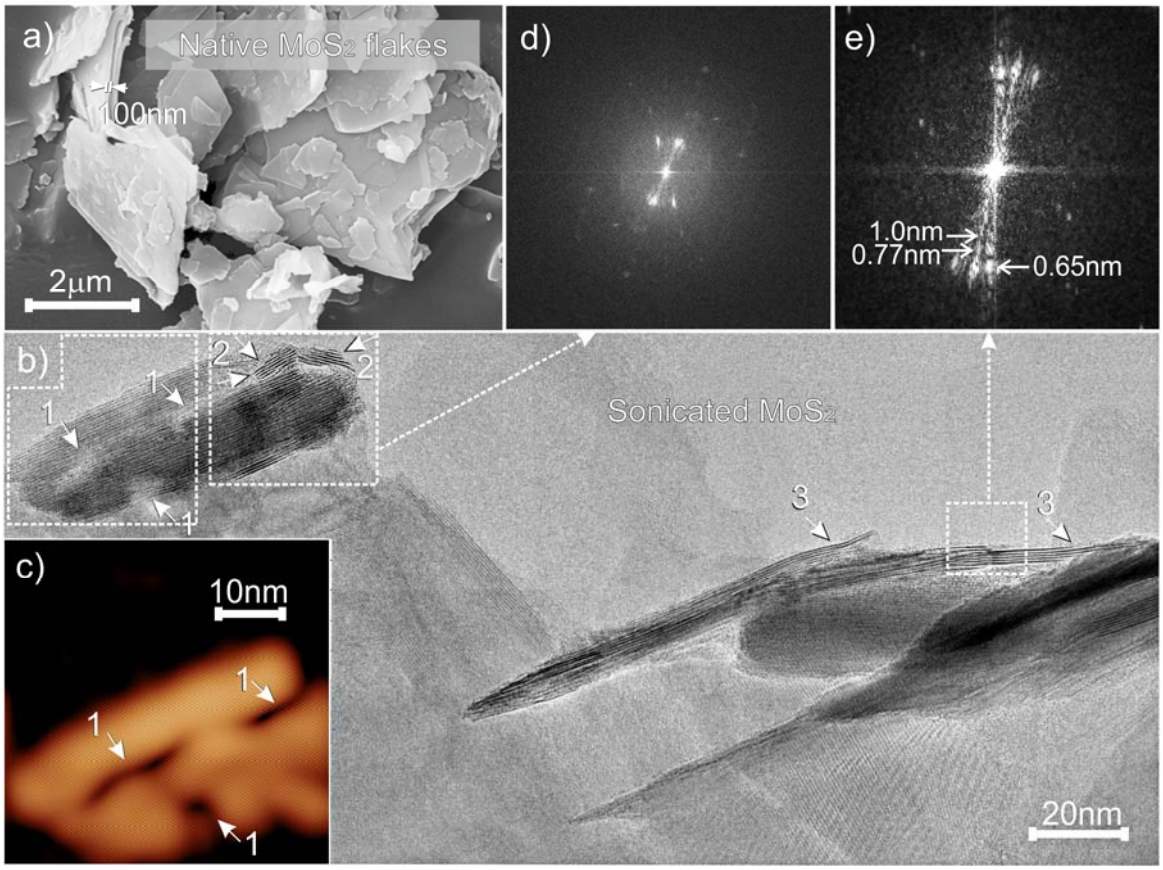

Figure 1. SEM image of native MoS_2 microflakes (a); HRTEM images of defective MoS_2 nanosheets after sonication (b); IFFT filtered image of the selected region in 1) (c); FFT images of the (2) and (3) selected regions (d and e) The white arrows indicate fractured (1, 2) or exfoliated regions (3) of nanosheets. The bright color of c) corresponds to the masked spots belonging to (002) interplanar distance of MoS_2, while the darker areas indicate the more defective regions.

The larger and thicker MoS_2 flakes extracted from the bottom of the supernatant solution are TEM imaged in Figure 1b. With respect to the native material, these multilayer flakes have size greatly reduced (from 0.5-5 μm to 60-250 nm). Also the average thickness is smaller (from about 100 to 10-30 nm). These results indicate that the particles extracted from the bottom of the solution, although having multilayer nature, are the result of a simultaneous exfoliation and fragmentation process. In other words, it is concluded that sonication in IPA, unlike higher boiling solvents cited above, is not solely favouring exfoliation. The structure of the fragments shown in Figure 1 merits a specific analysis because it gives information about the exfoliation/fragmentation mechanism. Three different regions have been selected:

1- border regions of a defective MoS_2 particle with locally interrupted fridges;

2- few-layer stacked ($\approx$5-6L) MoS_2 regions, 10 nm in size;

3- exfoliated and extended few-layer MoS_2 nanoplatelets.

More details about the (1) selected region, are shown in the color IFFT (Inverse Fast-Fourier Transform) filtered images (Figure 1c and Figure S3 Supporting Information, the color scale being here arbitrary). It results that, the dark regions are corresponding to the same observed from TEM image, with locally interrupted fringes. More information on the (2) smaller domains about 10 nm thick (medium red color) and on the (3) elongated regions are obtained from FFT (Fast-Fourier Transform) patterns shown in Figure 1d and 1e. The observed asymmetry of the reciprocal lattice points, is explained with a different confinement of the thin samples: few-layer MoS_2 nanoclusters (2) and more exfoliated and extended MoS_2 nanoplatelets (3).

The distinctive features observed in both electron beam diffraction patterns can then be used as a method for identifying single - multi layers or clusters – extended layers.

On the basis of the before discussed results, we can conclude that an intense cavitation field in isopropyl alcohol causes: i) a reduction of the layers number (exfoliation) due the breaking of the interactions between the planes of MoS_2 flakes, ii) a remarkable fragmentation perpendicularly to basal planes, thus breaking the Mo-S bonds and then promoting the occurrence of defective edges as well (*vide infra*); iii) the formation of numerous defects, which are interrupting the crystallographic symmetry.

3.2 Morphology and structure of the MoS_2 nanoparticles extracted from the transparent and opaque regions of the ultracentrifuged solution.

Mixtures of MoS_2 nanosheets/nanoparticles from the transparent and opaque fractions are TEM imaged in Figure 2a and 2c respectively.

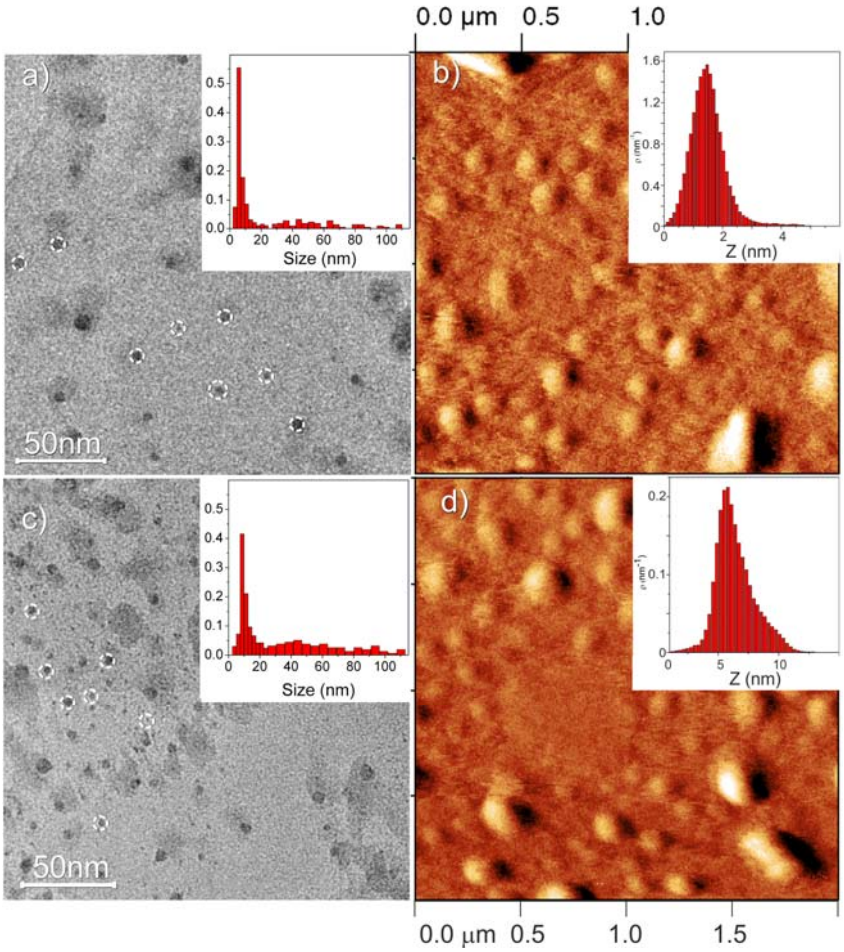

Figure 2. TEM (a, c), amplitude-signal AFM (b, d) images of the MoS_2 nanoparticles obtained from the"transparent" and from of the "opaque" fractions, respectively. White circles in a) and c) illustrate the smaller MoS_2 nanoparticles. Size distributions of the MoS_2 nanoparticles are shown in the inserts of a) and c) TEM images, while the height distributions are shown in the insert of b) and d) AFM images.

In Figure 2a, the majority of MoS_2 nanosheets (transparent fraction) has lateral sizes ranging in the 3-11 nm interval (small particles in circles in Figure 2a), with a small contribution of larger slabs about 25-40 nm in size (very thin platelets). Such distribution is illustrated in the histogram, (insert in Figure 2a). Most of the smallest particles are supported on larger platelets. This could be associated with particle agglomeration during solvent evaporation. Of course the large particles, although smaller in number, are likely dominating

in term of weight %. It will be shown that this fact has important consequences on the UV-Vis-NIR spectrum. In Figure 2c (opaque fraction), beside the high contribution of larger MoS_2 sheets, small slabs having size distributions with maxima in the 5-15 nm range are observed (histogram in the insert of Figure 2c). These results show that even the bad isopropyl alcohol solvent is efficient in exfoliation and fragmentation under sonication. While TEM images are mostly indicative of the particle size distribution, nothing can be inferred on the layer number of the particles at the adopted resolution. However, as the thickness of thin MoS_2 slabs can be usually obtained by atomic force microscopy (AFM),[29, 32, 54, 58-59] AFM images of particles deposited on mica from transparent and opaque solutions have been obtained. The height distributions of the MoS_2 nanosheets are shown in Figure 2b and 2d. MoS_2 nanosheets coming from the transparent fraction show a weight distribution centred between 1 and 3 layers (insert in Figure 2b). Conversely, MoS_2 nanosheets coming from the opaque fraction show a weight distribution centred between 3 and 10 layers (insert in Figure 2d). Notice that the lateral sizes obtained by AFM are overestimated. In fact the tip radius is about 10 nm, which is a value of the same order of magnitude of the features under estimation.

It is likely appropriate at this point to ask whether particles with size smaller than 1.5 nm and escaping TEM and SEM detection, are present after sonication. As particles with such small size should have optical properties approaching those of quantum dots, a discussion on this point is postponed to the paragraph where the optical properties are more specifically discussed.

More details on the structure of the particles, which are the main fraction of MoS_2 in transparent solutions, can be obtained with high resolution transmission microscopy (Figure 3ac).

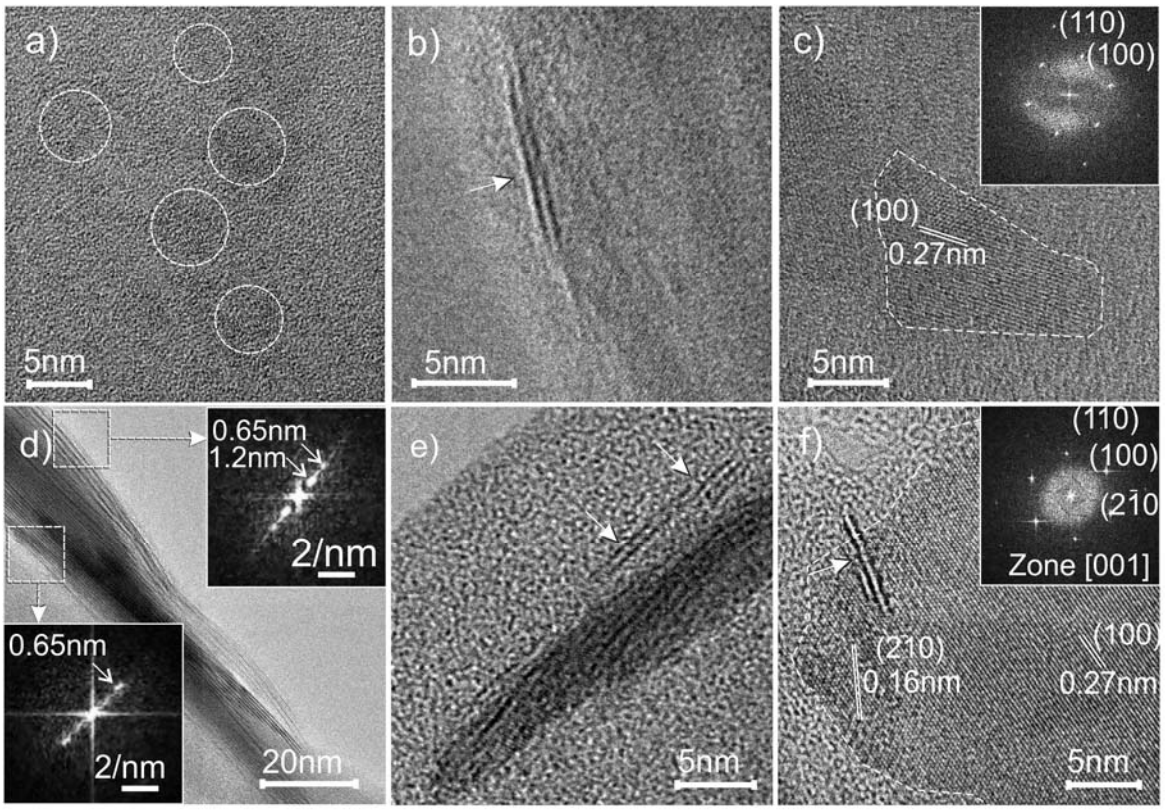

Figure 3. HRTEM images of MoS_2 nanosheets coming from the "transparent" (a, b, c) and from the "opaque" (d, e, f) fractions of the sonicated/centrifuged solutions. In Figure (a, b and c) very thin, two layers and monolayer MoS_2 nanosheets are shown. In Figure (d, e and f) large/thick and defective two/three layers thick MoS_2 nanosheets are illustrated. The dotted line in c) and in f) indicate small MoS_2 slabs, which are FFT imaged in the inserts therein.

From these figures, some thin slabs 3-10 nm in sizes (circles in Figure 3a), a single nanosheets two layers thick (about 8 nm in length) (Figure 3b) and a MoS_2 monolayer with irregular shape exposing lattice fringes 0.27 nm spaced, corresponding to (100) planes (Figure 3c) are HRTEM imaged.

A hexagonal symmetry of the MoS_2 is in agreement with the arrangement and spacing of the bright spots in the Fast Fourier Transform (FFT) image (insert of Figure 3c).[27] HRTEM images of MoS_2 nanosheets, coming from opaque solutions are illustrated in Figure 3d-f). Notice that more thick and elongated layers can be observed. In particular a relatively thick (~20nm) MoS_2 lamina, more than 100 nm in length, shows irregular terminations (Figure 3d). In fact, besides a first FFT image (bottom left insert) showing two bright spots, which are associated with 0.65 nm regularly spaced (002) planes, from the second FFT image (top-right insert), an additional and "unusual" couple of bright spots, 1.2 nm spaced, is observed due to more distant planes. Within the heterogeneity of our sample, smaller (5-10 nm) and even defective two/three layers

thick MoS_2 slabs, exposing (002) planes, are HRTEM imaged in Figure 3e,f. From Figure 3f (and insert therein) an irregularly shaped MoS_2 nanosheet, exposing {100} and {2-10} lattice fringes, 0.27 nm and 0.16 nm, respectively spaced, is oriented along the [001] zone axis, corresponding to the basal plane. Bright spots (on FFT image), associated with the {100} and {2-10} plane families, are confirming the hexagonal MoS_2 structure.[27]

In conclusion, from TEM images, it comes that MoS_2 nanosheets expose predominantly basal planes. Moreover, the low contrast of the images could be roughly indicative of the presence of "thin" MoS_2 nanosheets (either single or few stacked layers).

3.3 Lattice structures of mono and multilayers MoS_2.

One and multi-layers MoS_2 nanosheets with periodic lattices can be observed along the quite continuous and extended (tens of nm) film covering the copper grids (1L- MoS_2 in Figure 4 and MLs- MoS_2 in Figure S1 - Supporting Information).

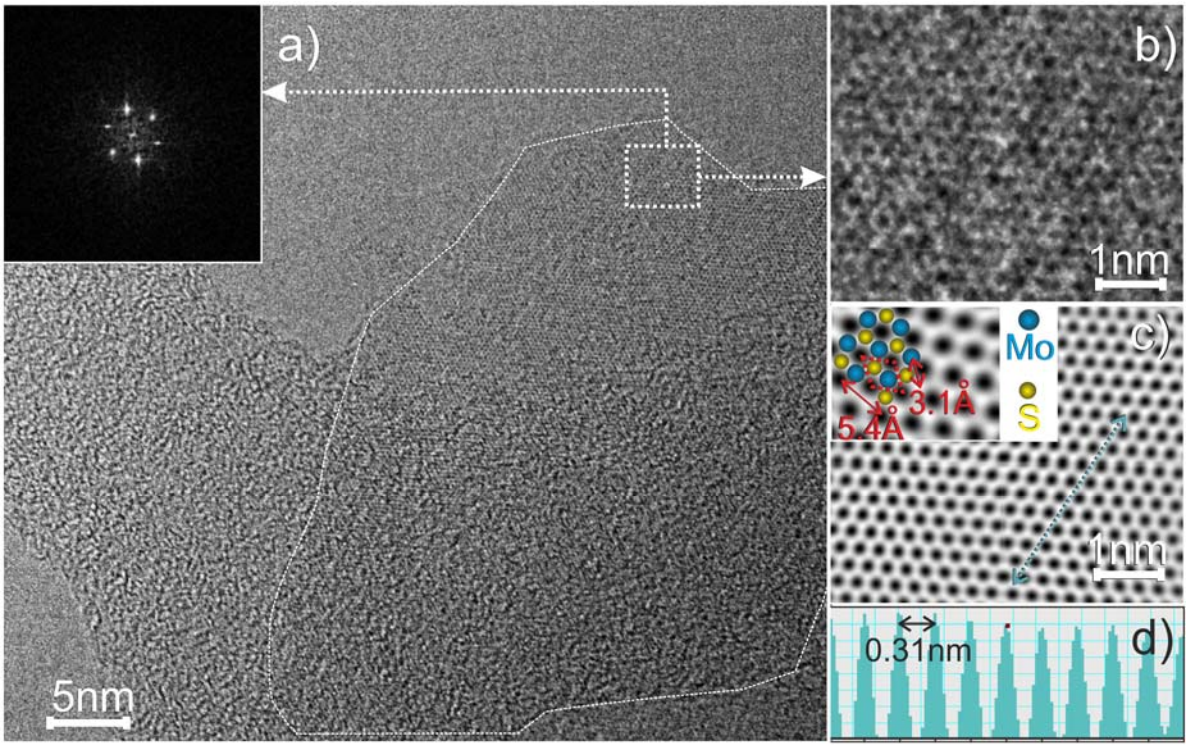

Figure 4. HRTEM image of a MoS_2single layer, extending over the lacey-carbon grid region (a); non-filtered (b) and IFFT-filtered atomic resolution selected area (c) of a portion of Figure (a); atomic spacing along the selected direction of the basal plane, as calculated for a MoS_2 single layer (d). In the insert of c), cell parameters calculated from the IFFT-filtered atomic resolution area are shown.

As far as the particle imaged on Figure 4 is concerned, the first-order diffraction spots of the FFT image (insert of Figure 4a) on a selected area are shown according to a regular hexagonal symmetry, thus indicating the presence of individual sheets made of single crystal domains, without fold-stacked regions (i.e. Moiré patterns).[26] Moreover HRTEM images of the selected area in a) before and after FFT filtering are shown in Figure 4b,c. From the IFFT filtered image (Figure 4c), showing a regular honeycomb pattern, due to the atomic arrangements of Mo and S atoms (identified by difference in their contrast),[15] the in-the-plane lattice constants of MoS_2 have been determined to be ~0.31 nm and ~0.54 nm, respectively. In Figure 4d, the calculated profile along the selected direction in Figure 4c is drawn. The 0.31 value is very close to that observed for exfoliated single-layer MoS_2,[26] whereas values about 0.315-0.32 nm have been found for bulk MoS_2.[29] Thus, no remarkable differences in the lattice parameters are expected for single, double and multilayer MoS_2 flakes. It is noteworthy that, by adopting suitable tilting operations, the layer number can also be revealed.[11] The FFT filtered image of 15x15nm areas (or 20x20nm) (Figure S2, Supporting Information) shows the presence of ripples (or isotropic corrugations, about 6-10 Å in height) with sizes of 6-10 nm along the plane of the nanosheets, thus indicating the presence of single layer MoS_2 (more flexible) with respect to MLs, which are significantly more flatten (i.e. in focus).[11] From comparison of the diffraction patters of mono and multilayers, the presence of reciprocal lattice rods, associated with each reciprocal lattice point is observed in case of 1L- MoS_2 (Figure S2, Supporting Information). The rods are more extended for the thinner samples than for the thicker ones, making it difficult to obey the Bragg condition when the samples are tilted. Bright spots, which are associated with the six-fold symmetry, but with different peculiar intensities, are obtained, in presence of ML- MoS_2 systems.[11]

*3.5 UV-vis spectroscopy***.**

In Figure 5, the UV-visible spectra of the three liquid fractions (a- highly diluted transparent, b- yellowish clear/transparent and c- more opaque gray liquid) are compared to that of the MoS_2 film, used as a reference (d) (absorptions at 679 nm, at 620 nm, at about 480 nm and at 399 nm). Curve (a) is the spectrum of 0.1 ml of sonicated solution taken from the topmost layer of the ultracentrifugation cuvette diluted into a cuvette

containing 4 ml of pure IPA solvent. Due the high dilution, the absorbance has been multiplied by a factor of 45.

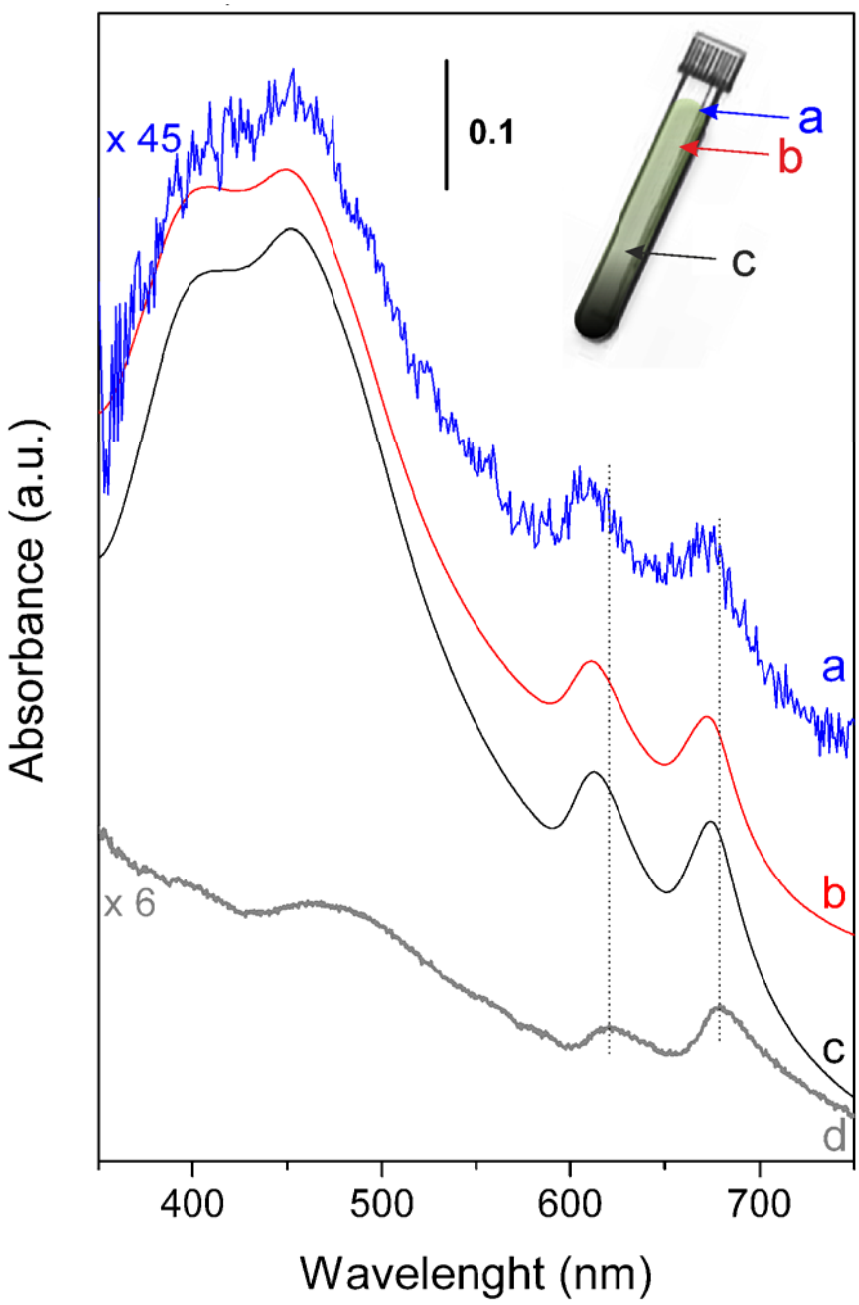

Figure 5. UV-vis spectra of the high diluted "transparent" (a), "transparent" (b) and "opaque" (c) fractions of sonicated MoS_2 in IPA, as compared to MoS_2 film dispersed on quartz used as a reference (d). Curve a) is the spectrum of 0.1 ml of sonicated solution taken from the topmost layer of the ultracentrifugation cuvette diluted into a cuvette containing 4 ml of pure IPA solvent. The spectrum has been magnified by a factor of 45.

On the basis of the literature data,[36] it comes that the spectral features of the reference MoS_2 (d) in Figure 5) can be assigned as follows: i) a first absorption threshold at about 700 nm due to a direct transition at the K point; ii) two sharp peaks at 679 nm and at 620 nm on the high energy side of this threshold due to A and B excitonic transitions, respectively, whose separation energy (about 59 nm) can be explained with spin-orbit splitting of the top of the valence band at the K point;[57, 60-62] iii) a second threshold, at about 500 nm, due to a direct transition from the deep in the valence band to the conduction band; iv) excitonic transitions (C and D) at 482 nm and at 399 nm, respectively, also associated with these threshold transitions; v) a third threshold at about 350 nm due to transitions from deep in the valence band.[57]

Two couples of bands for the opaque fraction are observed at 674 nm and at 613 nm (narrow, A and B excitons) and at 451 nm and at 410 nm (broad and intense envelope due to C and D excitonic transitions), whereas for the transparent fraction, the same couples are observed at 672 nm and at 611 nm (narrow, A and B excitons) and at about 449 nm and at 407 nm (C and D excitonic transitions). The situation emerging from spectrum (a) is very similar even if the A and B bands are further upward shifted. Notice that the energy values of the opaque fraction are in-between the film and the transparent fraction ones, but closer to the film ones. More exactly, in comparison to the reference values (MoS_2 film), the energy values of A and B excitons are only slightly upward shifted, whereas larger shifts are observed for C and D excitons, according to the fact that quantum size effects are affecting C and D bands in more remarkable way.

Furthermore, it has been experimentally shown[37] that the separation of the A and B bands is not greatly affected by the number of layers forming the (stoichiometric) MoS_2 particles. In fact, the position of the A and B peaks of single layers and bilayers are not sensibly different from the bulk. Conversely, a remarkable blue shift was obtained by some authors,[57] attributed to the quantum size effect in very small MoS_2 particles, behaving as quantum dots.

In conclusion, by comparing the spectra of the sonicated systems to that of the film, it is inferred that we are in the presence of a very moderate quantum size effects, thus indicating that the major fraction of MoS_2 particles does not reach a quantum dot state similar to that obtained by Wilcoxon et al.,[57] and that particles with size lower than 1.5 nm are not produced by sonication in IPA. It must however be underlined that a comparison between the results of this investigation and the results of ref *57*, where a sensible quantum size

effect was observed, must be taken with caution because the stoichiometry of MoS_2 dots prepared by bottom up method[57]is about 1/2.5. i.e. a figure quite far from the 1/2 Mo/S stoichiometry.

3.5 The vibrational spectrum of MoS_2 and the effect of edges functionalization as investigated by DRIFT.

As mentioned before, sonication induces layers separation and breaking. The two processes, which are occurring simultaneously, are schematically illustrated below (Scheme 1):

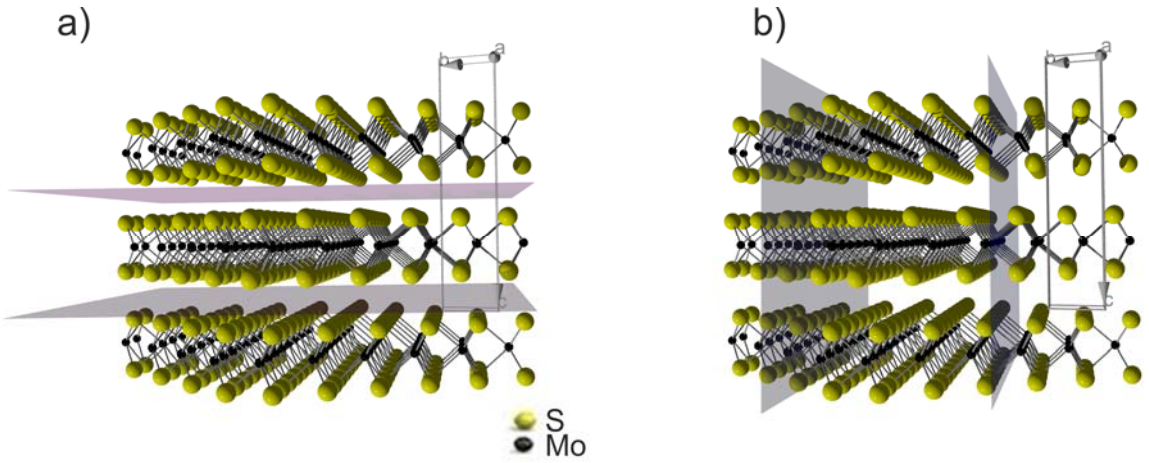

Scheme 1. Effects of the strong sonication of MoS_2 flakes dispersed in isopropyl alcohol: breaking between basal planes (a) and great fragmentation of lamellae (b).

We have documented that, while the effect of layers separation on the physical properties of MoS_2 has been widely investigated, the same is not true for layers fragmentation. We have so decided to investigate this point by means of DRIFT spectroscopy. This study has been stimulated not only by the TEM results illustrated before, but also by the contribution of Maugè *et al.*[63-64], who have shown by FTIR that the surface of MoS_2 particles and layers exposed to air are covered by various types of species, including sulphate groups. Although the location of these species was not fully specified by the previously mentioned papers, the involvement of the terminations, where the layers are broken and interrupted, is a probable explanation.

To investigate this problem the vibrational spectrum of MoS_2, before and after sonication for increasing time, has been investigated (Figure 6).

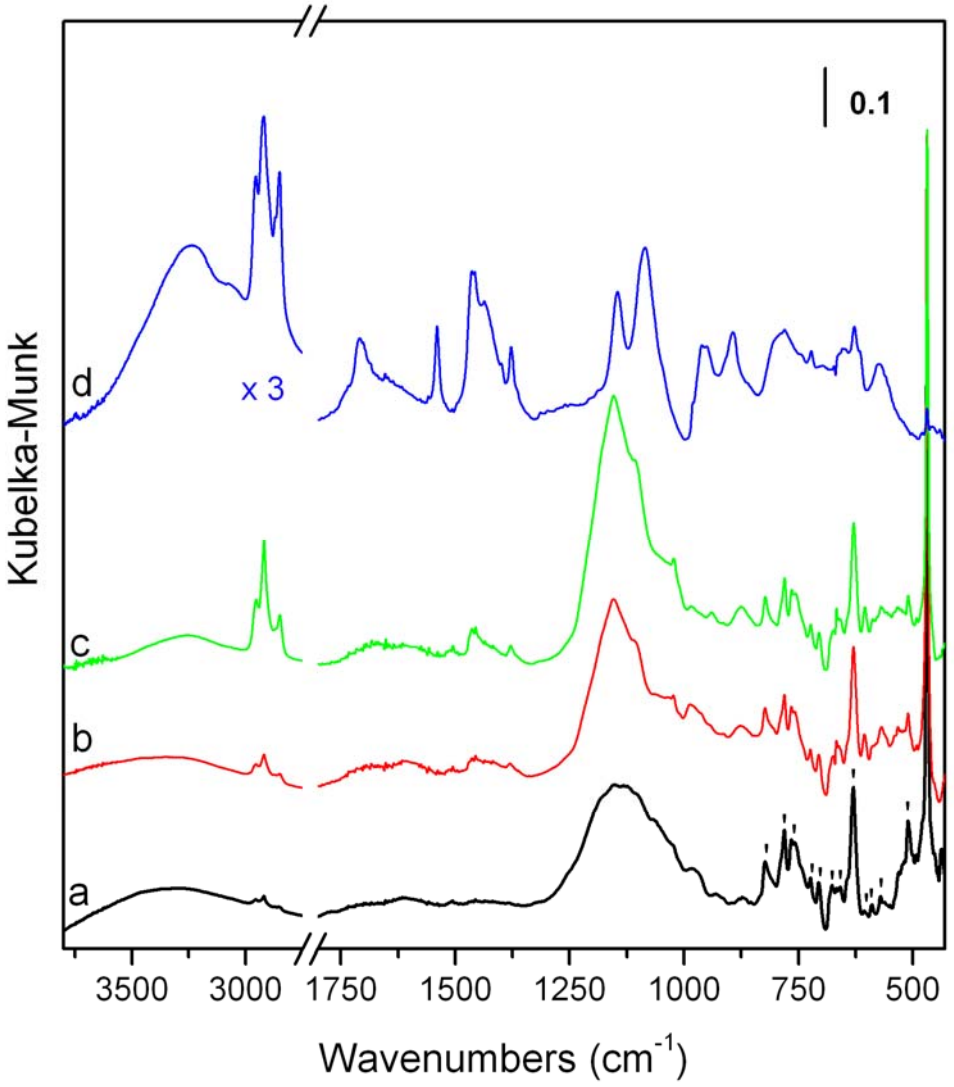

Figure 6. DRIFT spectra of bulk MoS_2 dried at 100°C (a); MoS_2 sonicated for 6 hours in IPA and dried at 100°C (b); MoS_2 sonicated for 18 hours in IPA and dried at 100°C (c). Combination and overtones of fundamental modes are indicated by (|). Spectrum d) has been obtained from the fraction extracted from the topmost layer of the ultracentrifugation cuvette. Due to the small amount of material the absorbance has been multiplied by 3.

The spectrum of virgin MoS_2 (Figure 6 curve a) is characterized by the vibrational manifestations of bulk solid as testified by the narrow and strong band at 469 cm^{-1}, which is the infrared active fundamental A_{2u} mode of MoS_2[65]. The very numerous, narrow and weaker bands in the 500- 850 cm cm^{-1} interval (509 cm^{-1}, 573 cm^{-1}, 588 cm^{-1}, 603 $cm^{-1,}$ 629 cm^{-1}, 665 cm^{-1}, 677 cm^{-1}, 705 cm^{-1}, 723 cm^{-1}, 764 cm^{-1},779 cm^{-1} and 822 cm^{-1}: indicated by |) merit a specific comment because they have never been reported in the literature and because they contain information on the multilayer character of the flakes of the virgin sample. To make an

assignment of these combinations and overtones of fundamental modes we remind that the vibrational representation of active modes in bulk and monolayers MoS_2 are as follows [66-67].

Γ(bulk MoS_2) = A_{2u} (IR) + E_{1u} (IR) + A_{1g} (R) + 2E_{2g} (R) +E_{1g} (R)

Γ (monolayer) = A''_2 (IR) + E' (IR + R) + A'_2 (R) + E" (R)

The two IR modes of bulk MoS_2, A_{2u} (469.4 cm^{-1}) and E_{1u}, (391.2 cm^{-1}) evolve into the IR-active A''_2 (490.5 cm^{-1}) and E' (402,7 cm^{-1}) of the monolayer representation, while the A_{1g} (R) (412 cm^{-1}) and E_{1g} (R) (288.7 cm^{-1}) evolve into A'_2 (R) (423 cm^{-1}) and E'' (R) (296 cm^{-1}). The E_{2g} (R) interlayer mode is absent in the Γ (monolayer) representation. These representations and the associated frequencies are valid for perfect crystals and perfect monolayers. In our case, due to the presence of a high concentration of defects and terminations, which are destroying the symmetry, it is expected that the Raman active modes can show some IR activity. It can be observed that the spectrum of the perfect monolayer is quite similar to that of the perfect multilayer crystal, the only difference being the shift of the bands at higher frequency (+10-15 cm^{-1}) and the absence of the interlayer mode at 35.2 cm^{-1}.[67-68] The experimental spectra of Figure 6 (curves a-c) shows an intense peak at 469 cm^{-1}, which is nearly coincident with the value reported by Cai et al. [67] for perfect multilayer MoS_2 structures. From this, it is inferred that the in sonicated solution a consistent fraction of multilayer particles is present in agreement with TEM and SEM observations.

Although many overtones and combination frequencies can be originated by the 469.4 cm^{-1}, 412 cm^{-1}, 391 cm^{-1}, 288 cm^{-1} intralayer modes (for instance A_{2u}+ A_{1g}, A_{2u}+ E_{1u}, A_{2u} + E_{1g}, 2 E_{1u}), the multitude of narrow bands observed in the experimental DRIFT spectrum of the virgin material cannot be fully explained without the intervention of the E_{2g} (R) interlayer mode at 35.2 cm^{-1}. In other words the fine structure of the vibrational spectrum in the 400-850 cm^{-1} range is another signature of the multilayer structure of the particles. As the fine spectroscopic structure is present also in the spectra of the samples after sonication, it is once more inferred that a very consistent fraction of particles have multilayer structure. Their narrow character is also showing that the responsible structures are relatively perfect. This result is in agreement with the results shown in Figure 2, showing that the major fraction of particles is characterized by about 5 nm size and constituted by 3-10 layers, and that larger particles are also present, which can account for a large weight percentage.

As the TEM image of Figure 2 shows clearly the presence of very small particles (both with single layer or few layer character) the question arises about the expected vibrational manifestations of these structures. Following Cai et al.[67] perfect and infinite single layers are characterized by frequencies about 15 cm^{-1} upward shifted. However, in the present case, we are in presence of truncated particles of variable size and shape. Hence a consistent broadening is expected to be present in the associated vibrational transitions. In particular, the fine structure due to overtones transitions should be absent.

That this is the case, it is demonstrated by the spectrum d), which has been obtained from the top most layer of the ultracentifugated solution, where very small nanoparticles of variable size are expected to be abundantly present. Indeed, in this spectrum the characteristic fine structure of perfect multilayered particles is nearly completely absent. In the 850-450 cm^{-1} range the bands are broad and ill defined in agreement with the high size and thickness dispersion. Furthermore, as it will be discussed in the following, the spectrum of MoS_2 nanoparticles is largely overshadowed by the modes of adsorbed species present at defects and terminations. Following Maugè et al.[63] the very strong and very abroad absorption in the 1150-1000 cm^{-1} range present in spectrum a) is mostly due to sulphate groups adsorbed on defect sites. This assignment indicates that virgin MoS_2 from Aldrich contains adsorbed impurities, presumably formed by oxidation of the surface and likely occurring at defect sites following the reaction:

$$(MoSMo + 2\ O_2 \rightarrow MoSO_4Mo)$$

Sonication for increasing times (curves b and c) has a strong effect on the DRIFT spectrum of MoS_2. In fact, the absorption in the 1150-1100 cm^{-1} range, together with smaller components at lower frequencies, increases, thus indicating that surface sulphate groups concentration is slightly increasing. A definitely stronger increment is observed also for the broad absorption centred at 3250 cm^{-1} (due to stretching modes of -OH groups) and for bands in the 2960-2850 cm^{-1} and 1460-1380 cm^{-1} ranges (due to the stretching and bending modes of $-CH_3$ and $-CH_2$ groups). A low intensity and broad band at about 1700 cm^{-1} suggests that also minor amounts of carboxylate and or carbonylic groups are also formed, plausibly by oxidation of alkyl groups.

As expected, the surface groups manifestations become dominating in spectrum d) corresponding to the smallest particles. In particular OH and alkyl vibrations become very intense and the signature of carboxylate/carbonylic groups absorbing in the 1450-1750 range (presumably associated with incipient

oxidation of alkyl groups) distinctly show up. The same does not hold for the sulphate groups band, which tend to decline.

Taken together these facts clearly demonstrate that sonication is accompanied by an increasing functionalization of the surface. As we have demonstrated by TEM, SEM and UV-vis spectroscopy that sonication is accompanied by extensive fragmentation, it can be inferred with confidence that these surface species, are located at the termination of the MoS_2 layers, and behave as probes of layers fragmentation. A plausible explanation of the abundant formation of hydroxyl and aliphatic groups and, to a less extent of carboxylate/ carbonylic groups deriving from the previous ones by incipient oxidation, can be given on the basis of the following series of reactions, which occurs at the positions, where the energetic cavitation induces the breaking of the MoSMo bonds (Scheme 2).

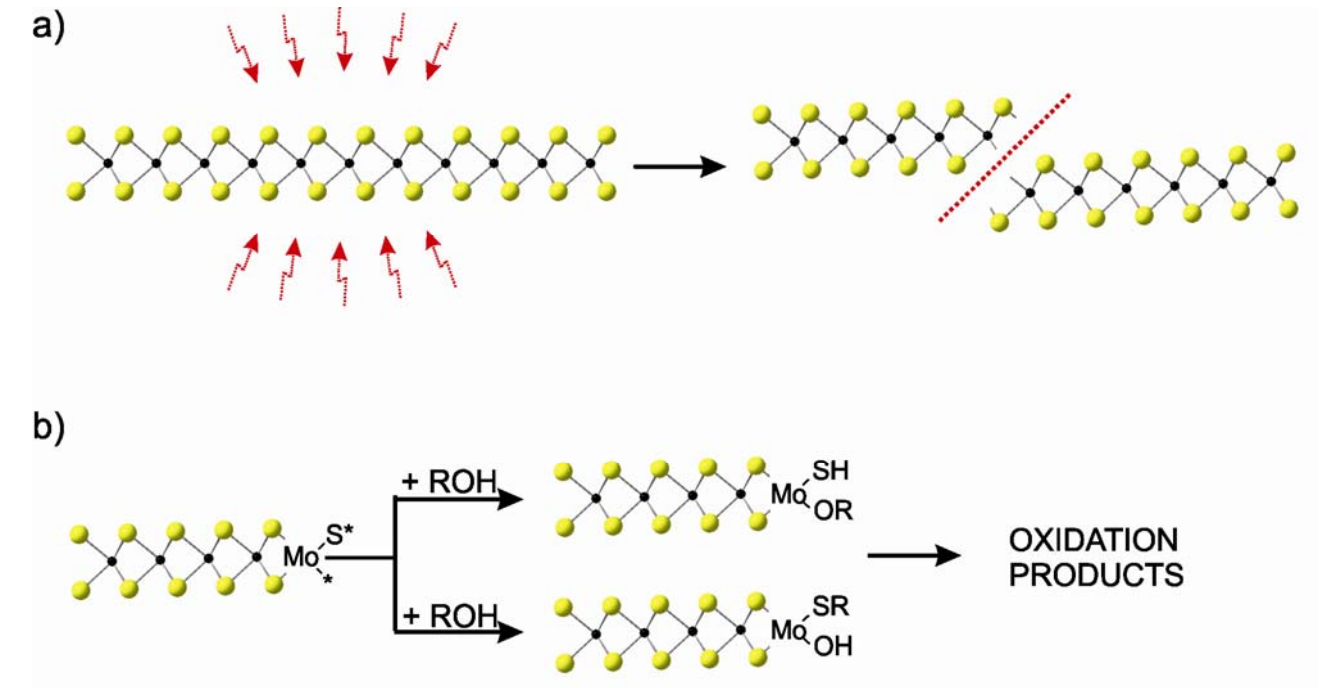

Scheme 2. Reactions, which may occur at the positions where the energetic cavitation induces the breaking of the MoSMo bonds (a), with predominant formation of hydroxyl, aliphatic groups. Carboxylate, carbonylic and sulphate species, particularly evident after prolonged treatment,are presumably deriving from the alkyl groups by incipient oxidation.

The coordinatively and chemically unsaturated groups, which are formed on steps likely interdependent, readily react with the solvent and with the oxygen of the atmosphere, so mainly causing the formation of

hydroxyl, alkyl groups described above. This process, when extended to small MoS_2 clusters containing a large fraction of coordinatively unsaturated surface atoms, necessarily leads to extensive surface functionalization. This means that very small MoS_2 clusters synthesized in solution cannot be considered as having the 1Mo:2S stoichiometry, because other atoms like oxygen, carbon and hydrogen are necessarily present in the same particle.

We underline that the reactions represented in the scheme have only indicative character, because other processes can be present on MoS_2 submitted to the highly energetic cavitation conditions, as testified by the formation of oxidized structures after prolonged sonication treatment. Furthermore, we cannot exclude that, beside layer terminations, also the basal surfaces can be partially involved and functioned.

Of course, the number and type of surface groups will depend on the solvent and on the amount of oxygen in the atmosphere. New efforts must be made to clarify all the aspects of the surface functionalization accompanying the cavitation. When the clusters are synthesized in presence of excess sulfur following a bottom up process (like made by Wilcoxon *et al.*[57]) the formation of non stoichiometric clusters containing excess of sulfur (in the form of $S\text{-}S_2^{=}$) is the necessary consequence.

4. Conclusions.

The sonication of MoS_2 dispersed in isopropyl alcohol has been adopted to obtain small and few-layer-thick MoS_2 nanoparticles. By investigating the obtained particles with AFM, TEM and HRTEM, the morphology, the structure in terms of lattice periodicity and formation mechanisms of nanosheets have discussed. In particular, it is shown that an intense cavitation field, when carried out in a small volume with a relatively poor solvent like isopropyl alcohol (IPA), makes possible to exfoliate and fragment thick flakes of stacked MoS_2 with the prevailing formation of thin sheets and particles with small lateral sizes comprised in a narrow interval (1.5-6 nm). This occurs via the great propagation of cracks perpendicular to basal planes. Although the dispersion is not stable for long time due to restacking phenomena and then sedimentation, the proposed method is suitable to prepare hybrid composite materials based on the simple impregnation of the high surface area support with the MoS_2 dispersion. The evolution of the UV-Vis-NIR and DRIFT spectra upon increasing sonication time and ultracentrifugation give unprecedented information on the optical properties of nanoparticles and on the vibrational properties of surface species and of the lattice modes of

virgin and fragmented material. It is demonstrated that, due to the cavitation field, the fragmentation of extensive layers leads to a rupture of MoSMo bonds and subsequent exposure of coordinatively and chemically unsaturated Mo and S species. These unsaturated chemical species readily react with the IPA solvent and to a less extent with atmospheric oxygen with the predominant formation of surface hydroxyl, alkyl and, in a lower degree, oxidized species like carbonylic and carboxylate groups. It is so concluded that the edges formed by layers breaking in the IPA solution are fully functionalized. The extensive funtionalization associated with particle breaking, which is covering the surface of aliphatic groups can have an indirect effect on particle solubility in IPA solvent and contribute to the whole colloid formation process. The detailed study of DRIFT spectra has allowed not only to obtain unprecedented information on the adsorbed species, but also on the vibrational modes of MoS_2 in the 400-850 cm^{-1} range and on their modification upon sonication. Finally the detailed analysis of the UV-Vis -NIR spectra has allowed to conclude that : i) quantum size effects have only small influence on the excitons spectra of MoS_2 particles with size larger than 1.5 nm; ii) the optical properties of MoS_2 particles prepared by sonication (top-down approach) cannot be compared in a straightforward way with MoS_2 quantum dots prepared by bottom-up approach in presence of excess sulfur.

AUTHOR INFORMATION

Corresponding Author

*Federico Cesano, e-mail: federico.cesano@unito.it, fax: + 39 011 6707855, ph: + 39 011 6707834

Author Contributions

The manuscript was written through contributions of all authors. All authors have given approval to the final version of the manuscript.‡These authors contributed equally. (match statement to author names with a symbol).

Funding Sources. This work was supported by MIUR (Ministero dell'Istruzione, dell'Università e della Ricerca), INSTM Consorzio and NIS (Nanostructured Interfaces and Surfaces) Inter-Departimental Centre of University of Torino.

References.

(1) Cravanzola, S.; Haznedar, G.; Scarano, D.; Zecchina, A.; Cesano, F., Carbon-Based Piezoresistive Polymer Composites: Structure and Electrical Properties. *Carbon* **2013**, *62*, 270-277.

(2) Haznedar, G.; Cravanzola, S.; Zanetti, M.; Scarano, D.; Zecchina, A.; Cesano, F., Graphite Nanoplatelets and Carbon Nanotubes Based Polyethylene Composites: Electrical Conductivity and Morphology. *Mater. Chem. Phys.* **2013**, *143*, 47-52.

(3) Castellanos-Gomez, A.; Poot, M.; Steele, G. A.; van der Zant, H. S. J.; Agraït, N.; Rubio-Bollinger, G., Elastic Properties of Freely Suspended MoS_2 Nanosheets. *Adv. Mater.* **2012**, *24*, 772–775.

(4) Dupont, C.; Lemeur, R.; Daudin, A.; Raybaud, P., Hydrodeoxygenation Pathways Catalyzed by MoS_2 and Nimos Active Phases: A Dft Study. *J. Catal.* **2011**, *279*, 276–286.

(5) Gaur, A. P. S.; Sahoo, S.; Ahmadi, M.; Guinel, M. J.-F.; Gupta, S. K.; Pandey, R.; Dey, S. K.; Katiyar, R. S., Optical and Vibrational Studies of Partially Edge-Terminated Vertically Aligned Nanocrystalline MoS_2 Thin Films. *J. Phys. Chem. C* **2013**, *117*, 26262−26268.

(6) Huang, X.; Zeng, Z.; Zhang, H., Metal Dichalcogenide Nanosheets: Preparation, Properties and Applications. *Chem. Soc. Rev.* **2013**, *42*, 1934-1946.

(7) Muratore, C.; Varshney, V.; Gengler, J. J.; Hu, J. J.; Bultman, J. E.; Smith, T. M.; Shamberger, P. J.; Qiu, B.; Ruan, X.; Roy, A. K., et al., Cross-Plane Thermal Properties of Transition Metal Dichalcogenides. *Appl. Phys. Lett.* **2013**, *102*, 081604.

(8) Ruinart de Brimont, M.; Dupont, C.; Daudin, A.; Geantet, C.; Raybaud, P., Deoxygenation Mechanisms on Ni-Promoted MoS_2 Bulk Catalysts: A Combined Experimental and Theoretical Study. *J. Catal.* **2012**, *286*, 153–164.

(9) Singh, N.; Jabbour, G.; Schwingenschlögl, U., Optical and Photocatalytic Properties of Two-Dimensional MoS_2. *Eur. Phys. J. B* **2012**, *85*, 392-395.

(10) Tongay, S.; Varnoosfaderani, S. S.; Appleton, B. R.; Wu, J.; Hebard, A. F., Magnetic Properties of MoS_2: Existence of Ferromagnetism. *Appl. Phys. Lett.* **2012**, *101*, 123105 - 123105-4.

(11) Brivio, J.; Alexander, D. T. L.; Kis, A., Ripples and Layers in Ultrathin MoS_2 Membranes. *Nano Lett.* **2011**, *11*, 5148–5153.

(12) Cesano, F.; Bertarione, S.; Piovano, A.; Agostini, G.; Rahman, M. M.; Groppo, E.; Bonino, F.; Scarano, D.; Lamberti, C.; Bordiga, S., et al., Model Oxide Supported MoS_2 Hds Catalysts: Structure and Surface Properties. *Catal. Sci. Technol.* **2011**, *1*, 123-126.

(13) Dellavalle, M.; Sandig, N.; Zerbetto, F., Stability, Dinamics and Lubrication of MoS_2 Platelets and Nanotubes. *Langmuir* **2012**, *28*, 7393-7400.

(14) Ding, S.; Zhang, D.; Chen, J. S.; Lou, X. W. D., Facile Synthesis of Hierarchical MoS_2 Microspheres Composed of Few-Layered Nanosheets and Their Lithium Storage Properties. *Nanoscale* **2012**, *4*, 95-98.

(15) Eda, G.; Yamaguchi, H.; Voiry, D.; Fujita, T.; Chen, M.; Chhowalla, M., Photoluminescence from Chemically Exfoliated MoS_2. *Nano. Lett.* **2011**, *11*, 5111-5116.

(16) Late, D. J.; Huang, Y.-K.; Liu, B.; Acharya, J.; Shirodkar, S. N.; Luo, J.; Yan, A.; Charles, D.; Waghmare, U. V.; Dravid, V. P., et al., Sensing Behavior of Atomically Thin-Layered MoS_2 Transistors. *ACS Nano* **2013**, *7*, 4879–4891

(17) Praveena, M.; Jayaram, V.; Biswas, S. K., Friction between a Steel Ball and a Steel Flat Lubricated by MoS_2

Particles Suspended in Hexadecane at 150 °C. *Ind. Eng. Chem. Res.* **2012**, *51*, 12321−12328.

(18) Savan, A.; Pflüger, E.; Voumard, P.; Schröer, A.; Simmonds, M., Modern Solid Lubrication: Recent Developments and Applications of MoS_2. *Lubr. Sci.* **2000**, *12*, 185–203.

(19) Shanmugam, M.; Bansal, T.; Durcan, C. A.; Yu, B., Molybdenum Disulphide/Titanium Dioxide Nanocomposite-Poly 3-Hexylthiophene Bulk Heterojunction Solar Cell. *Appl. Phys. Lett.* **2012**, *100*, 153901.

(20) Tye, C. T.; Smith, K. J., Catalytic Activity of Exfoliated MoS_2 in Hydrodesulfurization, Hydrodenitrogenation and Hydrogenation Reactions. *Top. Catal.* **2006**, *37*, 129-135.

(21) Wang, H.; Yu, L.; Lee, Y.-H.; Shi, Y.; Hsu, A.; Chin, M. L.; Li, L.-J.; Dubey, M.; Kong, J.; Palacios, T., Integrated Circuits Based on Bilayer MoS_2 Transistors. *Nano Lett.* **2012**, *12*, 4674−4680.

(22) Wang, T.; Gao, D.; Zhuo, J.; Zhu, Z.; Papakonstantinou, P.; Li, Y.; Li, M., Size-Dependent Enhancement of Electrocatalytic Oxygen-Reduction and Hydrogen-Evolution Performance of MoS_2 Particles. *Chem. Eur. J.* **2013**, *19*, 11939-11948.

(23) Wang, T.; Liu, L.; Zhu, Z.; Papakonstantinou, P.; Hu, J.; Liu, H.; Li, M., Enhanced Electrocatalytic Activity for Hydrogen Evolution Reaction from Self-Assembled Monodispersed Molybdenum Sulphide Nanoparticles on an Au Electrode. *Energy Environ. Sci.* **2013**, *6*, 625-633.

(24) Xiao, J.; Choi, D.; Cosimbescu, L.; Koech, P.; Liu, J.; Lemmon, J. P., Exfoliated MoS_2 Nanocomposite as an Anode Material for Lithium Ion Batteries. *Chem. Mater.* **2010**, *22*, 4522–4524.

(25) Zhou, W.; Yin, Z.; Du, Y.; Huang, X.; Zeng, Z.; Fan, Z.; Liu, H.; Wang, J.; Zhang, H., Synthesis of Few-Layer MoS_2 Nanosheet Coated Tio_2 Nanobelt Heterostructures for Enhanced Photocatalytic Activities. *Small* **2013**, *9*, 140-147.

(26) Ji, Q.; Zhang, Y.; Gao, T.; Zhang, Y.; Ma, D.; Liu, M.; Chen, Y.; Qiao, X.; Tan, P.-H.; Kan, M., et al., Epitaxial Monolayer MoS_2 on Mica with Novel Photoluminescence. *Nano Lett.* **2013**, *13*, 3870.

(27) Lee, Y.-H.; Zhang, X.-Q.; Zhang, W.; Chang, M.-T.; Lin, C.-T.; Chang, K.-D.; Yu, Y.-C.; Wang, J. T.-W.; Chang, C.-S.; Li, L.-J., et al., Synthesis of Large-Area MoS_2 Atomic Layers with Chemical Vapor Deposition. *Adv. Mater.* **2012**, *24*, 2320–2325.

(28) Najmaei, S.; Liu, Z.; Zhou, W.; Zou, X.; Shi, G.; Lei, S.; Yakobson, B. I.; Idrobo, J.-C.; Ajayan, P. M.; Lou, J., Vapour Phase Growth and Grain Boundary Structure of Molybdenum Disulphide Atomic Layers. *Nat. Mater.* **2013**, *12*, 754-759.

(29) Yu, Y.; Li, C.; Liu, Y.; Su, L.; Zhang, Y.; Cao, L., Controlled Scalable Synthesis of Uniform, High-Quality Monolayer and Few-Layer MoS_2 Films. *Sci. Rep.* **2013**, *3*, 1866.

(30) Frame, F. A.; Osterloh, F. E., Cdse-Mos_2: A Quantum Size-Confined Photocatalyst for Hydrogen Evolution from Water under Visible Light. *J. Phys. Chem. C* **2010**, *114*, 10628–10633.

(31) Goswami, N.; Giri, A.; Pal, S. K., MoS_2 Nanocrystals Confined in a DNA Matrix Exhibiting Energy Transfer. *Langmuir* **2013**, *29*, 11471–11478.

(32) Jeffery, A. A.; Nethravathi, C.; Rajamathi, M., Two-Dimensional Nanosheets and Layered Hybrids of MoS_2 and WS_2 through Exfoliation of Ammoniated Ms_2 (M = Mo,W). *J. Phys. Chem. C* **2014**, *118*, 1386−1396.

(33) Posudievsky, O. Y.; Khazieieva, O. A.; Cherepanov, V. V.; Dovbeshko, G. I.; Shkavro, A.; Koshechko, V. G.; Pokhodenko V. D., Improved Dispersant-Free Liquid Exfoliation down to the Graphene-Like State of

Solvent-Free Mechanochemically Delaminated Bulk MoS_2. *J. Mater. Chem. C* **2013**, *1*, 6411-6415.

(34) Quinn, M. D. J.; Ho, N. H.; Notley, S. M., Aqueous Dispersions of Exfoliated Molybdenum Dysulphide for Use in Visible-Light Photocatalysis. *ACS Appl. Mater. Interf.* **2013**, *5*, 12751.

(35) Wang, T.; Zhu, H.; Zhuo, J.; Zhu, Z.; Papakonstantinou, P.; Lubarsky, G.; Lin, J.; Li, M., Biosensor Based on Ultrasmall MoS_2 Nanoparticles for Electrochemical Detection of H_2O_2 Released by Cells at the Nanomolar Level. *Anal. Chem.* **2013**, *85*, 10289–10295.

(36) Wilcoxon, J. P.; Samara, G. A., Strong Quantum-Size Effects in a Layered Semiconductor: MoS_2 Nanoclusters. *Phys. Rev. B* **1995**, *51*, 7299-7303.

(37) Mak, K. F.; Lee, C.; Hone, J.; Shan, J.; Heinz, T. F., Atomically Thin MoS_2: A New Direct-Gap Semiconductor. *Phys. Rev. Lett.* **2010**, *105*, 136805.

(38) Ling, X.; Lee, Y.-H.; Lin, Y.; Fang, W.; Yu, L.; Dresselhaus, M. S.; Kong, J., Role of the Seeding Promoter in MoS_2 Growth by Chemical Vapor Deposition. *Nano Lett.* **2014**, *14*, 464−472.

(39) Wang, X.; Feng, H.; Wu, Y.; Jiao, L., Controlled Synthesis of Highly Crystalline MoS_2 Flakes by Chemical Vapor Deposition. *JACS* **2013**, *135*, 5304−5307.

(40) Clark, A.; Williams, R. H., The Optical Absorption Properties of Synthetic MoS_2. *J. Phys. D.* **1968**, *1*, 1222.

(41) Evans, L.; Young, P. A., Optical Absorption and Dispersion of Molybdenum Disulphide. *Proc. R. Soc. Lond. A* **1965**, *284*, 402-422.

(42) Frindt, R. F.; Yoffe, A. D., Physical Properties of Layered Structures: Optical Properties and Photoconductivity of Thin Crystals of Molybdenum Disulphide. *Proc. R. Soc. Lond. A* **1963**, *273*, 69-83.

(43) Shi, H.; Yan, R.; Bertolazzi, S.; Brivio, J.; Gao, B.; Kis, A.; Jena, D.; Xing, H. G.; Huang, L., Exciton Dynamics in Suspended Monolayer and Few -Layer MoS_2 2d Crystals. *ACS Nano* **2013**, *7*, 1072-1080.

(44) King, L. A.; Zhao, W.; Chhowalla, M.; Rileya, D. J.; Eda, G., Photoelectrochemical Properties of Chemically Exfoliated MoS_2. *J. Mater. Chem. A* **2013**, *1*, 8935-8941.

(45) Liu, L.; Qin, Y.; Guo, Z.-X.; Zhu, D., Reduction of Solubilized Multi-Walled Carbon Nanotubes. *Carbon* **2003**, *41*, 331-335.

(46) Wang, Y.; Ou, J. Z.; Balendhran, S.; Chrimes, A. F.; Mortazavi, M.; Yao, D. D.; Field, M. R.; Latham, K.; Bansal, V.; Friend, J. R., et al., Electrochemical Control of Photoluminescence in Two-Dimensional MoS_2 Nanoflakes. *ACS Nano* **2013**, *7*, 10083.

(47) Zeng, Z.; Yin, Z.; Huang, X.; Li, H.; He, Q.; Lu, G.; Boey, F.; Zhang, H., Single-Layer Semiconducting Nanosheets: High-Yield Preparation and Device Fabrication. *Angew. Chem. Int. Ed.* **2011**, *50*, 11093-11097.

(48) Coleman, J. N.; Lotya, M.; O'Neill, A.; Bergin, S. D.; King, P. J.; Khan, U.; Young, K.; Gaucher, A.; De, S.; Smith, R. J., et al., Two-Dimensional Nanosheets Produced by Liquid Exfoliation of Layered Materials. *Science* **2011**, *331*, 568-571.

(49) O'Neill, A.; Khan, U.; Coleman, J. N., Preparation of High Concentration Dispersions of Exfoliated MoS_2 with Increased Flake Size. *Chem. Mater.* **2012**, *24*, 2414.

(50) Yao, Y.; Tolentino, L.; Yang, Z.; Song, X.; Zhang, W.; Chen, Y.; Wong, C.-p., High-Concentration Aqueous Dispersions of MoS_2. *Adv. Funct. Mater.* **2013**, *23*, 3577.

(51) Cravotto, G.; Cintas, P., Sonication-Assisted Fabrication and Post-Synthetic Modifications of Graphene-Like Materials. *Chem. Eur. J* **2010**, *16*, 5246 – 5259.

(52) Cravotto, G.; Garella, D.; Calcio Gaudino, E.; Turci, F.; Bertarione, S.; Agostini, G.; Cesano, F.; Scarano, D., Rapid Purification/Oxidation of Multi-Walled Carbon

Nanotubes under 300 Khz-Ultrasound and Microwave Irradiation. *New. J. Chem.* **2011**, *35*, 915-919.

(53) Cunningham, G.; Lotya, M.; Cucinotta, C. S.; Sanvito, S.; Bergin, S. D.; Menzel, R.; Shaffer, M. S. P.; Coleman, J. N., Solvent Exfoliation of Transition Metal Dichalcogenides: Dispersibility of Exfoliated Nanosheets Varies Only Weakly between Compounds. *ACS Nano* **2012**, *6*, 3468-3480.

(54) Zhou, K.-G.; Mao, N.-N.; Wang, H.-X.; Peng, Y.; Zhang, H.-L., A Mixed-Solvent Strategy for Efficient Exfoliation of Inorganic Graphene Analogues. *Angew. Chem. Int. Ed.* **2011**, *50*, 10839-10842.

(55) Wang, K.; Wang, J.; Fan, J.; Lotya, M.; O'Neill, A.; Fox, D.; Feng, Y.; Zhang, X.; Jiang, B.; Zhao, Q., et al., Ultrafast Saturable Absorption of Two-Dimensional MoS_2 Nanosheets. *ACS Nano* **2013**, *7*, 9260-9267.

(56) Winchester, A.; Ghosh, S.; Feng, S.; Elias, A. L.; Mallouk, T.; Terrones, M.; Talapatra, S., Electrochemical Characterization of Liquid Phase Exfoliated Two-Dimensional Layers of Molybdenum Disulfide. *ACS Appl. Mater. Interfaces* **2014**, *6*, 2125−2130.

(57) Wilcoxon, J. P.; Newcomer, P. P.; Samara, G. A., Synthesis and Optical Properties of MoS_2 and Isomorphous Nanoclusters in the Quantum Confinement Regime. *J. Appl. Phys.* **1997**, *81*, 7934-7944.

(58) Firmiano, E. G. S.; Cordeiro, M. A. L.; Rabelo, A. C.; Dalmaschio, C. J.; Pinheiro, A. N.; Pereira, E. C.; Leite, E. R., Graphene Oxide as a Highly Selective Substrate to Synthesize a Layered MoS_2 Hybrid Electrocatalyst. *Chem. Commun.* **2012**, *48*, 7687–7689.

(59) Hwang, W. S.; Remskar, M.; Yan, R.; Kosel, T.; Park, J. K.; Cho, B. J.; Haensch, W.; Xing, H. G.; Seabaugh, A.; Jena, D., Comparative Study of Chemically Synthesized and Exfoliated Multilayer MoS_2 Field-Effect Transistors. *Appl. Phys. Lett.* **2013**, *102*, 043116.

(60) Abrams, B. L.; Wilcoxon, J. P., Nanosize Semiconductors for Photooxidation. *Crit. Rev. Solid State Mater. Sci.* **2005**, *30*, 153-182.

(61) Thurston, T. R.; Wilcoxon, J. P., Photooxidation of Organic Chemicals Catalyzed by Nanoscale MoS_2. *J. Phys. Chem. B* **1999**, *103*, 11-17.

(62) Wilcoxon, J. P.; Newcomer, P. P.; Samara, G. A.; Venturini, E. L.; Williamson, R. L. *Fundamental Science of Nanometer-Size Clusters*; Sandia National Labs. : Albuquerque, NM (USA), October 1995 1995; pp 19-30.

(63) Maugè, F.; Lamotte, J.; Nesterenko, N. S.; Manoilova, O.; Tsyganenko, A. A., Ft-Ir Study of Surface Properties of Unsupported MoS_2. *Catal. Today* **2001**, *70*, 271-284.

(64) Tsyganenko, A. A.; Can, F.; Travert, A.; Mauge, F., Ftir Study of Unsupported Molybdenum Sulfide - in Situ Synthesis and Surface Properties Characterization. *Appl. Catal. A* **2004**, *268*, 189–197.

(65) Dieting, T. J.; Verble, J. L., Infrared and Raman Studies of Long-Wavelength Optical Phonons in Hexagonal MoS_2. *Phys. Rev. B* **1971**, *3*, 4286-4292.

(66) Ataca, C.; Topsakal, M.; Aktürk, E.; Ciraci, S., A Comparative Study of Lattice Dynamics of Three- and Two-Dimensional MoS_2. *J. Phys. Chem. C* **2011**, *115*, 16354-16361.

(67) Cai, Y.; Lan, J.; Zhang, G.; Zhang, Y.-W., Lattice Vibrational Modes and Phonon Thermal Conductivity of Monolayer MoS_2. *Phys. Rev. B* **2014**, *89*, 035438.

(68) Rao, C. N. R.; Maitra, U.; Waghmare, U. V., Extraordinary Attributes of 2-Dimensional MoS_2 Nanosheets. *Chem. Phys. Lett.* **2014**, *609*, 172-183.

Optical, Vibrational and Structural Properties of MoS_2 Nanoparticles Obtained by Exfoliation and Fragmentation via Ultrasound Cavitation in Isopropyl Alcohol.

Lucia Muscus[a], Sara Cravanzola, Federico Cesano, Domenica Scarano and Adriano Zecchina.*

Department of Chemistry, NIS (Nanostructured Interfaces and Surfaces) Inter-Departmental Centre and INSTM Centro Di Riferimento, University of Torino, Via P. Giuria, 7, 10125 Torino (Italy).

Supporting Information (SI)

Additional HRTEM images and lattice parameters of MLs MoS_2, as obtained from the Inverse Fourier Transform (IFFT), are shown in Figure S1.

Inverse Fourier-Filtered images of single layer (1L) and multilayers (MLs) MoS_2, shown in Figure S2 a and 2b, respectively, have been obtained by means of a mask in Fourier Transforms of images. Remarkable variations of contrast (height differences) for 1L-MoS_2 are obtained in a small length scale (few nm), whereas smaller variation in height for MLs-MoS_2 are observed, because the planes are more flatten along the selected region and the material is more rigid [*Brivio, J., Alexander, D. T. L.; Kis, A. Nano Letters 2011, 11, 5148].*

HRTEM image of a defective MoS_2 nanoparticle after sonication and the obtained IFFT are shown in Figure S3. From these figures, it comes that the FTT processing allows to better individuate the defective regions indicated by the white arrows.

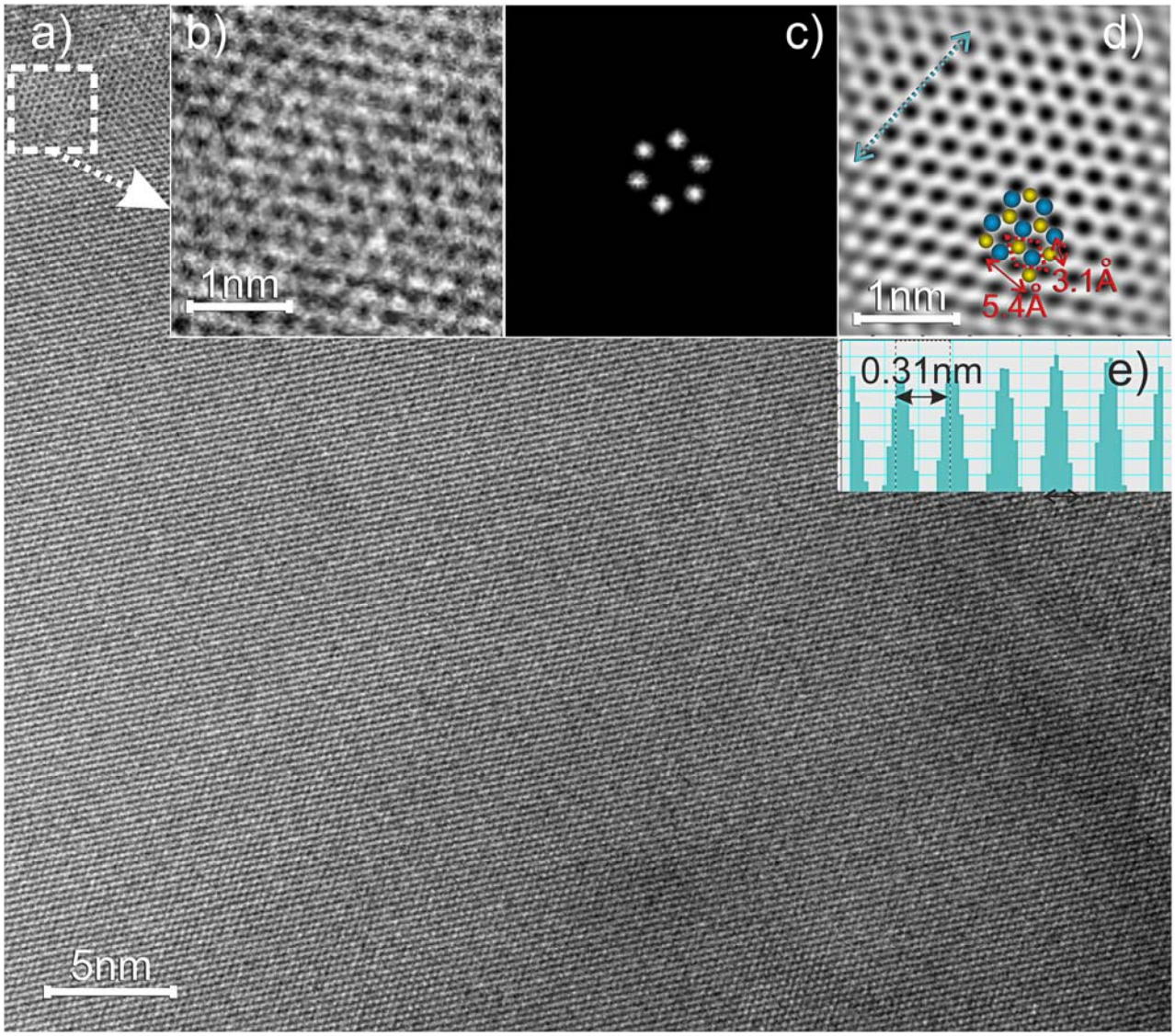

Figure S1. HRTEM image of a multilayer MoS_2 (a); HRTEM selected area (b) and FTT image (c) of the square region dotted in a); IFFT filtered image of the basal plane showing cell parameters (d); atomic spacing along the selected direction shown in d) (e).

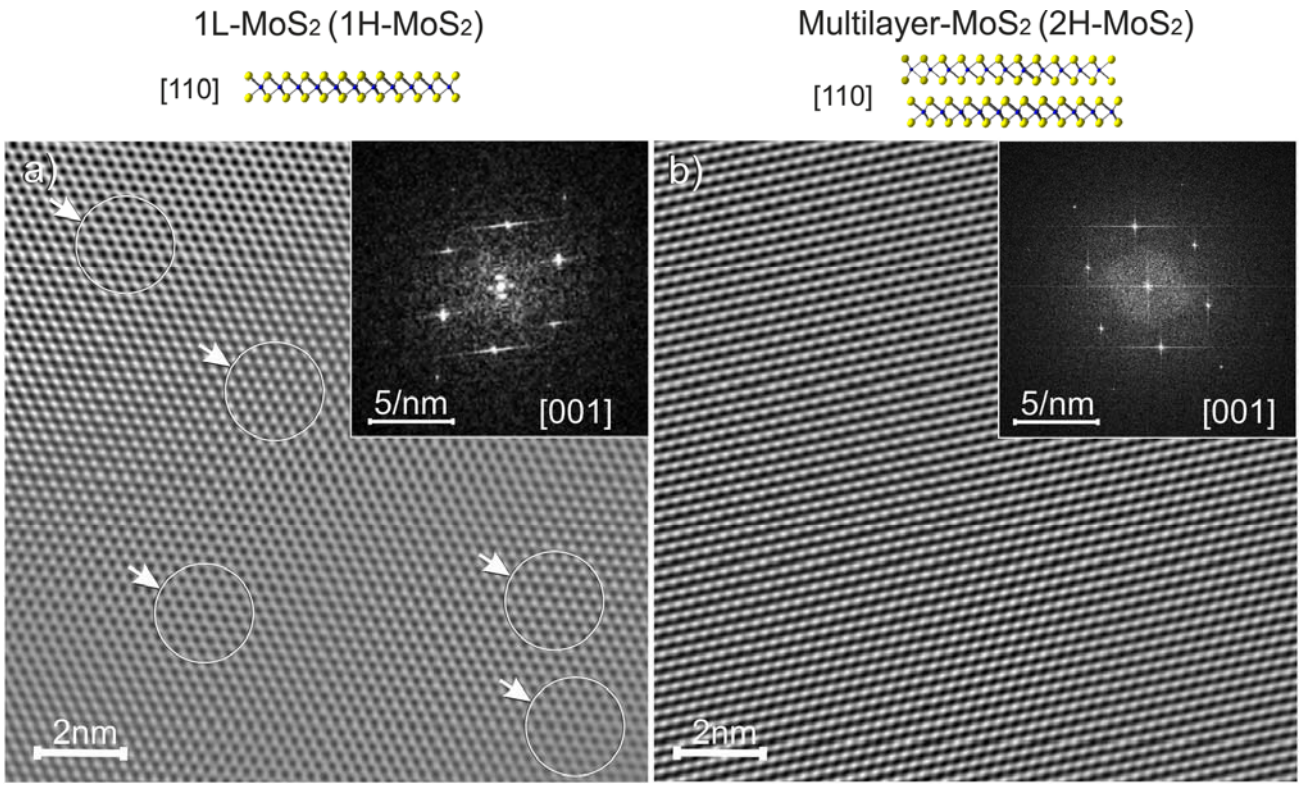

Figure S2. IFFT-filtered images (15x15nm) of a single layer (a) and of a multilayer MoS_2. (b). Regions with different contrast in a) are illustrated. In the inserts the two native FTT images are shown.

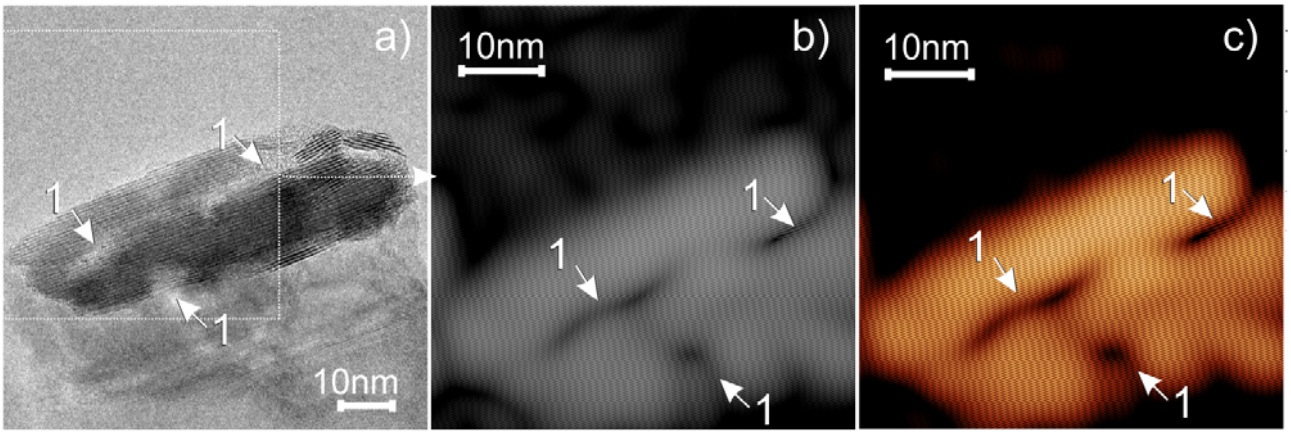

Figure S3. HRTEM image of a defective MoS_2 nanoparticle after sonication (a); white/black and color-like IFTT images (b and c) of the selected region in a); the white arrows indicate defective regions.